RSC Advances

ROYAL SOCIETY OF CHEMISTRY

www.rsc.org/advances

Graphical abstract

Donglin Li*, Hong-Tuan-Hua Yong, Rong Xie, Shoulong Ma, Miao Tian, Limin Hao, Xiaoyong Fan, Lei Gou, Lei Ni, Li Duan

Solution-processable design strategy for Li_2FeSiO_4@C/Fe nanocomposite as a cathode material for high power lithium-ion batteries

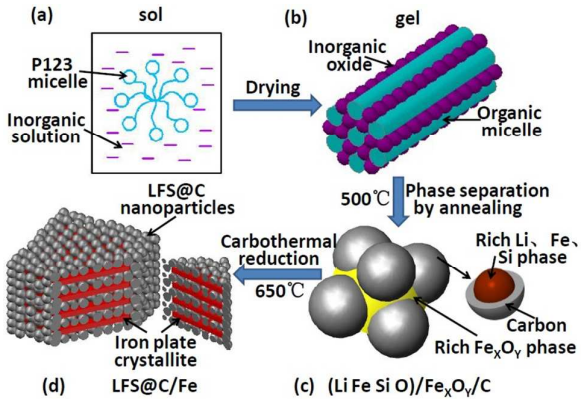

Li_2FeSiO_4@C/Fe nanocomposites have been synthesized by solution-processable approaches, which exhibits a superior rate performance.

Cite this: DOI: 10.1039/c0xx00000x

www.rsc.org/xxxxxx

ARTICLE TYPE

Solution-processabledesign strategy for Li_2FeSiO_4@C/Fe nanocomposite as a cathode material for high power lithium-ion batteries

Donglin Li*, Hong-Tuan-Hua Yong, Rong Xie, Xiaoyong Fan, Lei Gou, Miao Tian,Shoulong Ma, Limin Hao,Lei Ni, Li Duan

Received (in XXX, XXX) XthXXXXXXXXX 20XX, Accepted Xth XXXXXXXXX 20XX
DOI: 10.1039/b000000x

Li_2FeSiO_4@C/Fe nanocomposite has been synthesized by combining sol-gel and carbothermal reduction approaches. This process can be regarded as a general synthesis method for oxide-metal nanocomposite. Iron crystallites cansignificantly improve the high-rate performance of insulating oxide cathode materials for high-power lithium-ion batteries.

High performance lithium-ion batteries (LIB) are of great scientific and technological importance. Numerous applications call for higher specific capacities and fast charge-discharge rate for LIB. However, the most of electrode materials are electrical insulators which are one of the limitation steps of electrode kinetics.Nanoscale conductivity is crucial to high-rate performance of the electrode materials for energy conversion and storage devices.[1-2] The electronic conductivity of the electrode materials has been generally improved by carbon coating or decoration,[3-7] and cationic doping, [7-9] whereas an ionic transport is enhanced by nanostructuring electrode appropriately due to shortening the diffusion distance for lithium-ions as well as increasing effective interface area.[10-14] Of many approaches on improving conductivity of electrodes, graphene is regarded as an excellent conductive phase to constitute nanocomposites for high-power energy storage devices owing to its excellent electron mobility.[4] A lot of efforts have recently been focused on the development of graphene-nanocrystal composite cathodes.[3-6] However, it is difficult to ensure in-situ nucleation and growth of inorganic nanocrystals selectively on chemically derived graphene sheets due to the incompatibilities on synthesis processes of materials. Specially, it is difficult to control the particle size, uniform dispersion, and density of the loaded inorganic nanocrystals, as well as keeping the reduced graphene oxide sheets individually separated.[4-6]These pose significant limitations on the creation of useful graphene-based composites. Orthosilicate Li_2MSiO_4 (M =Fe, Mn, Co, Ni) compounds are promising electrode materials due to its theoretical capacity of 333 mAh g^{-1}.[15-17] Although a lot of reports have demonstrated that the Li_2FeSiO_4 (LFS) exhibits stable cyclability,[15-20] its application is still plagued by poor electrical conductivity (~10^{-14} S cm^{-1}) and low Li^+ diffusion coefficient (~10^{-16} cm^2 S^{-1}) that lead to rapid drop of rate capacity and large voltage fade.

Inspired by production of Sn-based composite by carbothermal reduction[21-22] and in-situ crystallization of SiO_2-based oxides,[20,23-25] we envisaged that nanoscale iron (0 valence Fe) could be produced by carbothermal reduction and used to design 'metal–oxide' composites. The target structure of a designed nanocomposite is shown in Scheme 1d, which is similar to the 'oxide nanocrystal-graphene' hybrid configuration.[4-6] The designed nanocomposite is composed of a large number of active LFS nanocrystals coated with amorphous carbon and smaller quantity of iron plate-like crystallites, which takes advantage of excellent electronic conductivity of metallic iron. In this communication, we report a solution-processable approach to synthesizeoxide@C-metalnanocomposite by using amphiphilic molecules as carbon source as well as template for forming mesopores. By controlling the composition of the precursor solution, mesoporous Li_2FeSiO_4@C/Fe nanocomposite with superior high-rate performances can be synthesized.

Scheme 1 Target structure and synthesis procedure of the materials.(a) The sol composed of P123 micelle and inorganic solution. (b) The hybrid gel composed of inorganic oxides and P123 organic micelles. (c) The oxides@C hybrid. (d) The designed Li_2FeSiO_4@C/Fe nanocomposite.

Our designing strategy for synthesizing such nanocomposites combines carbothermal reduction by which the iron can be produced, with in-situcrystallization of multicomponent oxide,[22-25] in which both iron and LFS nanocrystals can be controlled. The idea is that the organic carbon source is combined with at least two kinds of inorganic components using a sol–gel method to produce an organic–inorganic hybrid(ESI). After the organic fragments have been carbonized through annealing process, an inorganic oxide@C solid will be produced. Subsequent carbothermal reduction will force desirable nanocrystals to nucleate and to in-situ grow bycontrolling the temperature and duration of annealing processes, as schematically illustrated in Scheme 1.

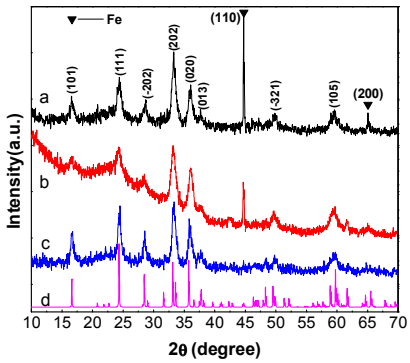

Fig. 1 XRD patterns of Li_2FeSiO_4@C/Fenanocomposites annealed at (a) 680 ℃ and (b) 650℃. (c) Li_2FeSiO_4@C sample annealed at 650℃. (d) ICSD#246132 pattern of Li_2FeSiO_4.

The triblock copolymers P123, which could be served as a structure directing agent for nanopores and a carbon source, was used to control LFS@C particles at thenanoscale and to introduce nanopores into the material. Fig. 1 shows XRD patterns from the synthesized materials. Primary reflection peaks can be indexed to a monoclinic structure with a space group $P2_1/n$ according to the results reported by Nishimura et al.[26] The LFS nanocrystals is approximately 7±3 nm in size according to Scherrer method from (111), (202) and (020) reflections for the sample annealed at 650℃. The narrow peaks at 44.7° and 65.1° belongs to larger α-Fe crystallites (Fig. 1b), suggesting crystalline phases consisted of dominant LFS nanocrystals and a smaller amount of Fe crystallites. When annealed at 680℃, the reflection intensity of the α-Fe crystallites becomesstronger, indicating the α-Fe content increases.

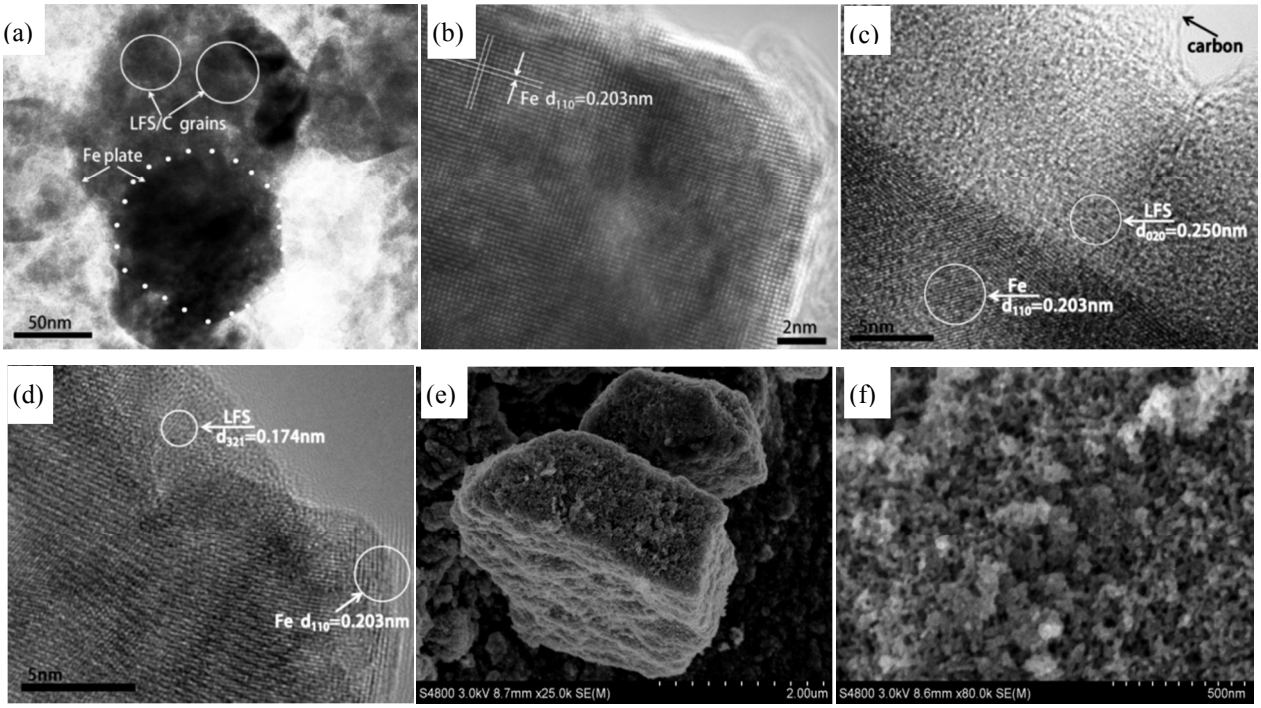

Fig.2 Electronic microscopy images of the Li_2FeSiO_4@C/Fe annealed at 650℃. (a) TEM image of Li_2FeSiO_4@C/Fe plates. (b) HRTEM images of a {110} <001>α-Fe plate nanocrystal. (c, d) HRTEM images of Li_2FeSiO_4@C/Fe plates.(e)FESEM image showing layer-like particles. (f) Enlargement of the surface of particle in the (e) image.

There are two kinds of particles in transmission electronic microscopy (TEM) images for the material, the larger plate-like one with size of 50–200 nm and smaller one with size of 4–20 nm. The most of the latter is anchored on the larger particles with polyhedral shape (Fig. 2a). High resolution TEM (HRTEM) analyses show that the larger plate-like particles are iron crystallites, showing lattice fringes with basal distances of 0.203 nm, corresponding to (110) plane of α-Fe crystal (Fig. 2b). The smaller particles are composed of LFS nanocrystals andamorphous carbon (Fig.2c). Dense and overlapped nanocrystals exhibit moiré pattern in the HRTEM image (Fig. 2d), indicating LFS nanocrystals anchored on Fe crystallites. The interface between the LFS and Fe crystals exhibits ordered lattices, implying the Fe crystallites incorporate together with the LFS nanocrystals. It indicates that a smaller amount of the Fe nanocrystals can intergrow and coexist with the LFS nanocrystals. It can be concluded that the material is composed of smaller size (approximately 5–10 nm) LFS nanocrystals, amorphous carbon, and Fe crystallites with a larger size from a few nanometers to sub-micrometers. The amorphous carbon layer with a thickness of 2 to 5 nm is coated on the surface of the LFS nanoparticles, forming LFS@C nanoparticles.

Field emission scanning electron microscope (FESEM) images of the LFS@C/Fe (Fig.2e) show micrometer size sandwich-like assemblages. Energy dispersive X-ray spectroscopy (EDS) shows higher Fe content compared to LFS@C (Figs. S1 and S2),indicating that the micometer assemblages possess a sandwich-like structure consisted of LFS@C nanoparicle layers and submicrometer Fe plate-like crystallites. A magnified FESEM image (Fig.2f) clearlyreveals that a large number of LFS@C nanoparticles with a size of 5–20 nm are uniformly dispersed on the surface of layer-like microparticles, forming disordered mesopores. In order to further confirm the larger size Fe plates in the interior of LFS@C/Fe

mcroparticles, the sample is further annealed at 680℃ for coarsening, as shown in the XRD pattern (Fig. 1a). As a result, bare Fe plate-like crystallites approximately 1–4μm in 2D size are clearly visible due to their Oswardripening and phase separationduring a annealing (Fig. S3). FESEM image clearly reveals a hint of layered construction in coarsening plate-like Fe crystallites (Fig.S3(a, b)).

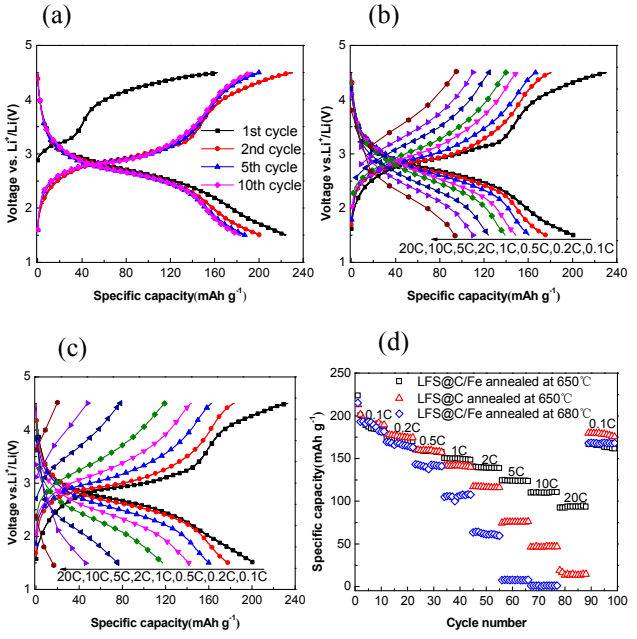

Fig.3 Charge/discharge performances of the materials in the voltage window of 1.5~4.5V. (a) charge/discharge voltage profiles of the Li_2FeSiO_4@C/Fe annealed at 650℃ at 0.1 C, (b,c) charge/discharge voltage profiles of the (b) Li_2FeSiO_4@C/Fe and (c) Li_2FeSiO_4@C compositesannealed at 650℃ at different rates, (d) rate cycling performances of Li_2FeSiO_4@C and Li_2FeSiO_4@C/Fe samples.

The formation mechanism of the LFS@C/Fe nanocomposite is associated with nano-phase separation of SiO_2-based multicomponent oxides.[20,23-25]When the organic carbon source P123 is converted to an amorphous carbon at 500℃, multicomponent oxides produces phase separation at the nanoscale, forming both nano-sized （Li, Fe, Si）phase (SiO_2-rich) and Fe_xO_y-rich phase during heating, whereas the amorphous carbon resides near rich-Si phase because the P123 assembles easily with amorphous silica. LFS nuclei nucleate in the amorphous SiO_2-rich phase during further heating. With increasing annealing temperature up to 650 ℃, the LFS nuclei grow in-situ into nanocrystals. Since the LFS nanocrystals are coated in-situ by the amorphous carbon, it is difficult to further grow into larger crystallites. During in-situ crystallization of LFS nanocrystals, an excess of Fe_xO_y-rich phase is defined the boundary between LFS@C nanoparticles, which is reduced in-situ into plate-like iron crystallites by carbothermal reduction, as schemitically illustrated in Fig. 1. Because smaller amount of the Fe_xO_y is defined on the boundaries of LFS@C nanoparticle, the carbothermal reduction results in thin iron layers which grow in 2D direction during crystallization, leading to sandwich-like LFS@C/Fe nanocomposite. Further annealing at 680℃ makes the iron layers grow into sub-micrometer plates at expense of tiny iron nanocrystals, resulting in bare larger Fe crystallites (Fig.1a, Fig.2(b, c), and Fig. S3). Thickness of Fe plates is plausibly estimated to approximately 10 to 50 nm according to FESEM and TEM observations (Fig. 2, Fig. S3b).

Fig. 3a shows the charge/discharge voltage profiles of several early cycles for the LFS@C/Fe composite with amorphous carbon content of approximately 12.9wt%at 0.1C (1C=166 mA g^{-1}). The LFS@C/Fe delivers an initial discharge capacity of approximately 218 mAh g^{-1} with little fading in the 2nd、5th and 10th cycles that deliver a discharge capacity of 207mAhg^{-1}, 193 mAhg^{-1} and 190 mAh g^{-1}, respectively. Considering iron content, the actual capacity of active LFS should be higher than the measured data, because it is difficult to determine the iron content in the LFS@C/Fe composite. The initial charge capacity is obviously lower compared with second cycle. It can be ascribed to smaller amount of delithation in active LFS nanocrystals due to incomplete filtration of the electrolyte into LFS@C/Fe particles. After the first cycle, the most of LFS@C/Fe particles are wetting with electrolyte, thus the charge capacity increased to 230 Ahg^{-1} in second cycle. Also, the electrochemical polarization of the cathode decreases, the Fe^{2+}/Fe^{3+} redox plateau return from initial 3.0–3.5 V to 2.8V during charge process. It indicates that the electrode kinetics is improved because the electrolyte is gradually filled into the inner particles. The second cycle exhibits still an approximately 4.3V voltage plateau corresponding to the Fe^{3+}/Fe^{4+} redox couple, implying lithiation/insertion of more than one lithium ions, in agreement with the capacity of higher than 166 mAh g^{-1}.

In order to demonstrate improved high-rate performances, the electrochemical performances of the LFS@C/Fe were compared with those of the LFS@C nanocomposite with similar morphology and LFS nanocrystals (Fig.2(e, f) and Fig. S2). The LFS@C/Fe shows a similar cyclability to the LFS@C at lower rates below 1C. Interestingly, the LFS@C/Fe shows significantly improved high-rate cycling performance at same conditions from 2C to 20C compared to LFS@Cnanocompositewith amorphous carbon content of approximately 16.5wt%. As increasing C-rates, the LFS@C/Fe exhibits smaller voltage hysteresis than the LFS@C. For example, the discharge plateau voltages fade toward lower potential for the LFS@C/Fe materials due to kinetics-limitation at high current rates (Fig.3b), while the LFS@C exhibits more rapid drop of the plateaus voltage(Fig.3c). Specifically, the flat plateau disappears at 20 C for the LFS@C, while it is obviously distinguished for the LFS@C/Fe. As a result, the LFS@C/Fe nanocomposite delivers a higher energy than the LFS@C at high rates. These results imply that the Fe crystallites decrease the electrochemical polarization in the LFS@C/Fe compared with the LFS@C, indicating that the electron transport kinetics is improved in the LFS@C/Fe cathode.

The LFS@C/Fe exhibits a superior rate capability. Fig. 3d shows the rate performances of the LFS@C/Fe and LFS@C cathodes. The two electrode thicknesses were designed to be same, so that thickness effects on rate performance could be ignored. Although both materials exhibit similar capacity retention with a gradual capacity fading at charge-discharge rates of 0.1–0.5 C, while the discharge capacity of the LFS@C/Fe becomes all along higher than the LFS@C at higher rates from 1C. Surprisingly, the capacity of the LFS@C drops dramatically from 2 C when the C-rates are increased up to 1–20 C, while the LFS@C/Fe exhibits gradual fading of capacity with increasing C-rates. Specially, a high reversible capacity of 108 mAh g^{-1} is retained after 80 cycles at 10 C for the LFS@C/Fe, which corresponds to a capacity loss only 1.0 % per cycle from initial discharge capacity of 183 mAh g^{-1} in 10th cycle at 0.1 C, corresponding to capacity retention of 59 %. In contrast, the discharge capacity of the LFS@C drops dramatically from 187 mAh g^{-1} in the 10that 0.1 C to 47 mAh g^{-1} at 10 C, which suffers a capacity fading rate of 2.0 % per cycle, a capacity retention of 25 %. Upon further increasing the current rate to 20C, the

discharge capacity of the LFS@C/Fe drops from 108 mAh g^{-1} at 10 C to 87 mAh g^{-1}, while the LFS@C drops dramatically from 47 to 20 mAh g^{-1}. Obviously, the capacity retention of the LFS@C/Fe cathode upon prolonged cycling is significantly improved over the LFS@C at high-rates. Indeed, the Fe crystallite in the composite plays a direct role of significantly improving high-rate charge/discharge performance by comparing the above charge-discharge and rate capability tests between LFS@C/Fe and LFS@C nanocomposites. It should be noticed that the rate performances of the LFS cathode is sensitive to distribution and morphology of Fe crystallites and LFS@C nanoparticles. As shown in Fig. 3 (c,d), the rate performance dramatically decays for LFS@C/Fe composite annealed at 680℃, because the bare Fe crystals with a larger size have almost lost effectively bridging conduction functionality due to separation of LFS@C and iron crystallites from the sandwich structure or coarsened larger particles free of nanopores(Fig. S3).

The superior high–rate performance of the LFS@C/Fenanocomposite benefits from the Fe plate-like crystallites. According to rate and cycling test, it can be deduced that both nanoporosity and 3D self-bridged carbon-iron conduction networks play a synergistic role on improving rate performance. First, the nanoporous sponge-like LFS@C particle can facilitate electrolyte permeating into the micrometer sized particle, thus providing an access and reservoirs for impregnating electrolyte into LFS particles as well as larger interface area between active nanocrystals and electrolyte that improve Li^+ transport rate in the cathode. Second, since the poor contact between loose packed LFS@C nanoparticles during contraction–expansion cycles, an electron transport is limited by the interface between the nanoparticles.[27] The Fe plates not only serve as protective spacers to prevent the agglomeration of LFS@C nanoparticles, but also act as 2D conducting sheet bridges approximately sub-micrometers in size to facilitate fast electron transport. In contrast, single carbon coating layer is hard to retain good conduction networks due to poorly electrical contact derived from contraction–expansion (charge-discharge) cycles. Thus major role of the Fe plates is to construct highly efficient electron conduction 2D areas/paths in the micrometer particles, significantly improving the electron transport flux and hence enhancing high-rate performance of LFS cathodes.

From all of the above discussions, it is clear that the introduction of the iron plates into LFS material dramatically alters the electrode kinetics. The Li_2FeSiO_4@C/Fe nanocomposites with stable cyclability and superior rate capability have been successfully fabricated by a sol-gel process. The comparison of electrochemical performance of the Li_2FeSiO_4@C/Fe and Li_2FeSiO_4@C nanocomposites proves that the Fe plate plays important roles not only in preventing the growth of Li_2FeSiO_4@C nanoparticles during material synthesis, but also in improving 2D electronic conduction area/path in the interior of Li_2FeSiO_4@C/Fe particles. The iron decrease the internal resistance by bridging electronically all the Li_2FeSiO_4@C particles and forming an optimal fast conducting network together with amorphous carbon in the entire electrode, hence enhance the electrochemical properties of Li_2FeSiO_4. We believe that this novel kind of Li_2FeSiO_4@C/Fe with ultrafine Li_2FeSiO_4@C homogeneously dispersed on Fe plates is a promising designed cathode material for high-power lithium-ion batteries. As an example of rationally controlled synthesis of metal-oxide composite, the solution-processable approach to such composites suggests a potentially general strategy to make other cathode materials. These results highlight that the design of metal-oxide heterogeneity could represent an important approach for manipulating electrode kinetics for high power lithium-ion batteries.

Notes and references

[a] *New Energy Materials and Device Laboratory, School ofMaterials Science and Engineering, Chang'an University, Xi'an, 710064, China*
Fax: 862982337340; Tel: 862982337350;
E-mail: donglinli@hotmail.com
†Electronic Supplementary Information (ESI) available: See DOI: 10.1039/b000000x/

1 J.Du, X.Lai, N.Yang, J.Zhai,D.Kisailus, F.Su, D.Wang and L.Jiang, *ACS Nano*, 2011, **5**, 590−596.
2 D.Liu and G.Cao, *Energy Environ. Sci*., 2010, **3**, 1218–1237.
3 H.Liu, G.Yang, X.Zhang, P.Gao, L.Wang, J.Fang, J.Pinto and X.Jiang,*J. Mater. Chem.*, 2012, **22**, 11039–11047.
4 D.Wang, R.Kou, D.Choi, Z.Yang, Z.Nie, J.Li, L. V.Saraf, D.Hu,J.Zhang, G. L.Graff, J.Liu, M. A.Pope and I. A.Aksay, *ACS Nano*, 2010, **4**,1587–1595.
5 X.Y.Fan, X.Y.Shi, J.Wang, Y.X.Shi, J.J.Wang, L.Xu, L.Gou and D.L.Li, *J. Solid State Electrochem*., 2013, **17**, 201-208.
6 H.Bai, C.Li and G.Shi, *Adv. Mater.* 2011, **23**, 1089–1115.
7 H.Hao, J.B.Wang, J.L.Liu, T.Huang and A.S.Yu, *J. Power Sources,* 2012, **210**, 397−401.
8 S. Y.Chung, J. T.Bloking and Y. M.Chiang, *Nat. Mater*. 2002, **1**, 123−128.
9 A. R.Cho, J. N.Son, V.Aravindan, H.Kim, K. S.Kang, W. S.Yoon, W. S.Kim and Y. S.Lee, *J. Mater. Chem.*, 2012, **22**, 6556–6560.
10 D.Li, M.Tian, R.Xie, Q.Li, X.Y. Fan, L.Gou,P.Zhao, S. L. Ma, Y. X. Shi and H.-T.-H.Yong, *Nanoscale,* 2014,**6**, 3302–3308.
11 J. H. H.Piku, G.Zhang, J.Cho, P. V.Braun and W. P.King,*Nat. Commun*, 2013, doi: 10.1038/ncomms2747.
12 S.Lee, Y.Cho, H.-K.Song and K. T.Lee, *Angew. Chem. Int. Ed.*, 2012, **51**, 8748–8752.
13 H.Zhou, D.Li, M.Hibino and I.Honma, *Angew. Chem. Int. Ed.*, 2005, **44**, 797−802.
14 C.Yuan , H. B. Wu, Y.Xie, and X. W. Lou , *Angew. Chem. Int. Ed.*, 2014, **53**, 1488–1504.
15 H.T.Zhou, M.Einarsrud and V.B.Fride, *J. Power Sources*, 2013, **235**, 234-242.
16 J.Y.Bai, Z.L.Gong, D.P.Lv, Y.X.Li,H. Zou and Y.Yang, *J. Mater. Chem.* 2012, **22**, 12128-12132.
17 R.Dominko, *J. Power Sources*, 2008, **184**, 462-468.
18 X.Y.Fan, Y.Li, J.J.Wang, L.Gou,P.Zhao, D.L.Li, L.Huang and S.G.Sun,*J. Alloys Comp*., 2010, **493**, 77-80.
19 W. Chen, M. Lan, D. Zhu, C. Ji, X. Feng, C. Yang, J. Zhang and L. Mi, *J. Mater. Chem. A*, 2013, **1**, 10912-10917.
20 D.Li, R.Xie, M.Tian, S.Ma, L.Gou, X.Fan, Y.Shi, H.-T.-H.Yong and L.Hao, *J. Mater. Chem. A*, 2014, **2**, 4375-4383.
21 G.Derrien,J.Hassoun,S.Panero andB.Scrosati, *Adv. Mater*. 2007, **19**, 2336-2340.
22 J. Wang, D. L. Li, X. Y. Fan, L.Gou, J. J. Wang, Y.Li, X. T. Lu and Q.Li, *J. Alloys Compd.,* 2012,**516**, 33– 37.
23 D.Li,H.Zhou and I.Honma,*Nat. Mater.*, 2004, **3**, 65−72.
24 D.Li,L.Kong, L.Zhang and X.Yao, *J. Non-Cryst. Solids,* 2000, **271**, 45–55.
25 D.Li, M.Tian, R.Xie, Q.Li, S.Ma, Y.Shi, F.Li, H. Lin, L.Gou, X. Y. Fan, P.Zhao, X.Wang and X.Yao, *J. Alloys Compd*. 2014, **582**, 88–95.
26 S.I.Nishimura, S.Hayase, R.Kanno, M.Yashima, N.Nakayama and A. Yamada, *J. Am. Chem. Soc.*, 2008, **130**, 13212–13213.
27 J.-Y.Kim and N. A.Kotov,*Chem. Mater*, 2014, **26**, 134–152.